The 16th International Congress on the Chemistry of Cement 2023 (ICCC2023)
"Further Reduction of CO_2 -Emissions and Circularity in the Cement and Concrete Industry"
September 18–22, 2023, Bangkok, Thailand

Kinetics of iron (hydr)oxide precipitation in cementitious materials

F.E. Furcas[1*], S. Mundra[1], B. Lothenbach[2], O.B. Isgor[3] and U.M. Angst[1]

[1] *ETH Zürich, Zürich, Switzerland,*
Email: ffurcas@ethz.ch, shishir.mundra@ifb.baug.ethz.ch, ueli.angst@ifb.baug.ethz.ch
[2] *Empa, Concrete & Asphalt Laboratory, Dübendorf, Switzerland*
Email: barbara.lothenbach@empa.ch
[3] *Oregon State University, Corvallis, OR, USA*
Email: burkan.isgor@oregonstate.edu

ABSTRACT

The accumulation of corrosion products throughout the concrete pore network may lead to the development of internal stresses and spalling of the concrete cover, thus facilitating further structural detonation. To gain a more profound understanding of this self-sustaining sequence of events, both the type of corrosion product(s) as well as their rate of formation within the chemical environment characteristic to cementitious materials must be investigated. By employing a combination of time-resolved TGA, XRD, XAS and ICP studies, we show that the formation of the thermodynamically stable end member goethite (α-FeOOH(s)) is preceded by rapid precipitation of 2-line ferrihydrite (2l-Fe(OH)3(s)) at alkaline pH. Over time, dissolution of the amorphous intermediate prompts re-crystallisation of goethite from solution. Here, precipitation rates scale with the H^+ activity. Kinetic rate laws deduced from the progression of aqueously dissolved iron and the amount of solid phase(s) present at any time can lead to better reactive transport models that predict the service life of reinforced concrete structures more accurately.

KEYWORDS: *Precipitation, nucleation, kinetics, pH, thermodynamic modelling,*

1. Introduction

Cementitious pore solutions contain a variety of dissolved species adding up to an ionic strength of up to 1.5 (Albert, Isgor et al. 2022). Their high alkalinity as well as the presence of silica, sulphates and carbonates make up for a unique set of crystallisation conditions for iron (hydr)oxide corrosion products that may favour the formation of amorphous intermediate phases over those that are thermodynamically stable (Schwertmann and Cornell 2008). Whilst a variety of studies investigate the formation of iron oxides at acidic, circumneutral and mildly basic pH (Schwertmann, Friedl et al. 1999, Schwertmann, Stanjek et al. 2004, Zhu, Frandsen et al. 2016), no attempt has been made to characterise the type of corrosion products stabilised at a pH greater than 12. This study shows that the two main corrosion products formed at alkaline pH are 2-line ferrihydrite (2l-$Fe(OH)_3$(s)) and goethite (α-FeOOH(s)). Here, rapid precipitation of 2l-$Fe(OH)_3$(s) dictates the solubility limit of iron within the first minutes of equilibration. Over time, re-dissolution of the amorphous intermediate prompts the precipitation of α-FeOOH(s) from solution. As goethite features a comparatively low specific molar volume compared to any other iron (hydr)oxide phase initial stabilisation of 2-line ferrihydrite may severely impact the evolution of internal stresses and thus the structural degradation over time.

The precipitation of solid Fe(III) (hyrd)oxides from solution can be formulated according to the general reaction

$$Fe^{3+} + (r + s)H_2O(l) \rightleftharpoons FeO_r(OH)_s^{3-2r-s} + (2r + s)H^+. \quad (1)$$

Whilst there are a range of analytical techniques at disposal to characterise the type and amount of solid corrosion product formed and monitor the coinciding drop in the aqueous Fe^{3+} concentration, a systematic investigation of the kinetic mechanism leading up to the formation of $FeO_r(OH)_s^{3-2r-s}$ remains challenging. This is due to a number of reasons. Firstly, even though only a few iron (hydr)oxides are thermodynamically

stable within the Fe-H-O system, many others precede the formation of their energetically more favourable counterparts or are shown to be stable at nanoscale (Soltis, Feinberg et al. 2016, Furcas, Lothenbach et al. 2022). Secondly, the solubility limit, as dictated by the dissolution e.g. α-FeOOH(s) is low (~10^{-8} M at pH 13.0) and differs from that of the more soluble iron hydroxide phases by more than 4 orders of magnitude (Wieland, Miron et al. 2023). Moreover, Fe^{3+} concentration in equilibrium with α-FeOOH(s) is significantly lower than that of other elements (Si, Na, K) commonly present in cementitious pore solutions. As some of the latter elements are frequently taken up by 2-line ferrihydrite (Thomas Arrigo, Mikutta et al. 2014) or inhibit the growth of other high stability iron phases (Rzepa, Pieczara et al. 2016), the aqueous matrix can severely impact the relative amounts of corrosion products stabilised as well as the measurement of the dissolved iron itself. Lastly, in-situ XAS measurements estimate time for iron (hydr)oxide precipitation to be in the orders of microseconds at room temperature. Given the already low solubility limit of ferric iron at alkaline pH, the limit of detection (LOD) of many measurement devices at disposal to quantify the total amount of dissolved iron is surpassed rapidly after reaction initiation (Caruso, Mantellato et al. 2017). Any attempt to measure the progression of aqueously dissolved iron over time requires a precise, matrix-matched calibration across the entire concentration range observed.

2. Materials and methods

To investigate the type and amount of corrosion product(s) stabilised at alkaline pH, three supersaturated iron stock solutions at pH 13.0, 13.5 and 14.0 have been prepared by dissolving $FeCl_3 \cdot 6H_2O$ in HNO_3. The acidic iron source was subsequently mixed with concentrated NaOH to achieve the desired final pH and a final Fe^{3+} concentration of 20 mM across all experiments conducted. The aqueous iron concentration was monitored over time by means of ICP-OES. Solids precipitated through the course of the reaction were centrifuged out and immediately freeze dried for two days and stored as dry powders to prevent further phase transition (Schwertmann, Friedl et al. 1999). Minerals were characterised using TGA and XRD within a time span of 30 days.

2.1. ICP-OES

Previous to ICP analysis, aliquots extracted from supersaturated iron stock solution were filtered and re-dissolved in 2 wt. % HNO_3 to prevent further precipitation. Measured signal intensities are related to the the total amount of aqueously dissolved iron by an 8-point calibration at concentrations ranging from 50 to 0.01 ppm. To capture above mentioned matrix effects and avoid spectral interference due to other elements present, four spectral lines of iron, namely 234.340, 238.204, 239.563 and 259.940 nm are considered. The level of detection (LOD) and quantitation (LOQ) of the device utilised is determined by following the recommendations of Caruso, Mantellato et al. (2017).

2.2. TGA

Powders extracted from supersaturated iron stock solution were heated from 303 to 1273 K at a rate of 10 K min^{-1}. Obtained TGA and DTG curves were compared to those of pure iron (hydr)oxide reference components and the conversion of one phase to another determined by means of the tangential method (Scrivener, Snellings et al. 2016).

2.3. XRD

X-ray diffractograms were measured on the interval between 4˚ to 80˚ in steps of 0.02 2θ using Co Kα radiation using a Bruker D8 Advance diffractometer. Crystalline phases stabilised over the timespan investigated are identified by comparing the obtained diffractograms to those of 2- and 6-line ferrihydrite, lepidocrocite, goethite, hematite and magnetite.

3. Results

DTG curves of the iron phases extracted from aged stock solutions feature two distinct peaks at ~100˚C and ~250 ˚C. Whilst the majority of water lost occurs within the first region of interest at early equilibration times, the second, high temperature peak is significantly more prominent in the long term samples. This is evident from Figure 1. Comparison to the derivative thermogravimetry signals of 2-line ferihydrite (2l-

$Fe(OH)_3(s)$), lepidocrocite (γ-FeOOH(s)) and goethite (α-FeOOH(s)) suggests that an FeOOH-type iron hydroxide is stabilised from 2-line ferrihydrite over time.

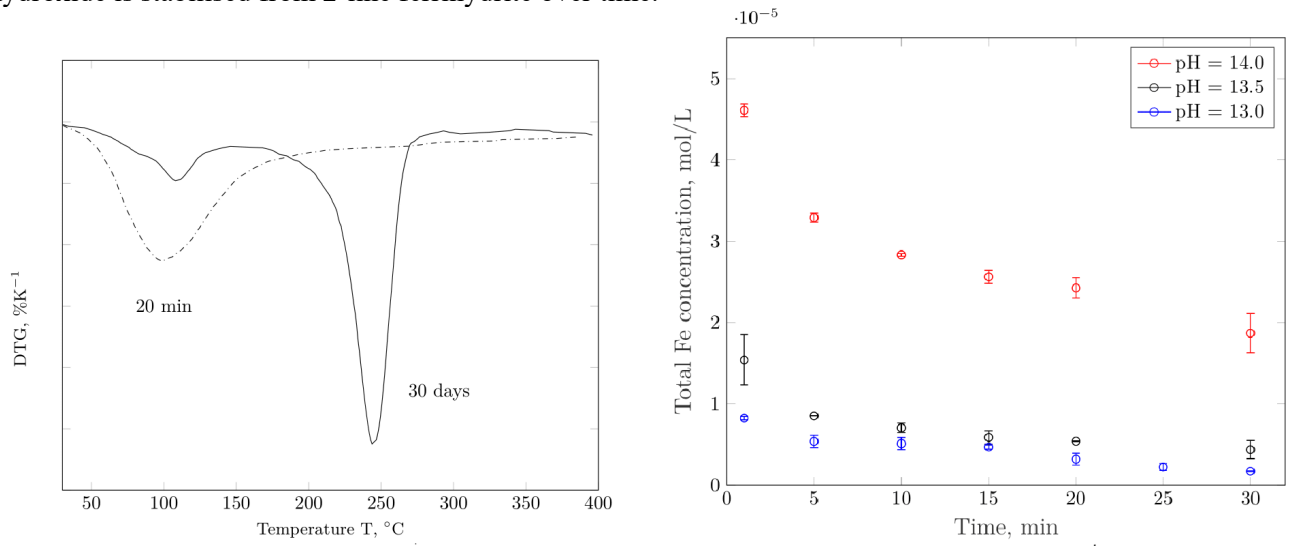

(a) (b)

Figure 1: DTG curves of solid iron phases extracted from supersaturated iron stock solutions (Subfigure 1a) together with the total aqueous iron concentration, as measured by ICP-OES at the spectral line of 259.940 nm (Subfigure 1b).

X-ray diffractograms further support this hypothesis and identify the FeOOH-type phase formed to be goethite. Aqueous iron concentrations in equilibrium with the mixture of solid phases stabilised decrease surpass the solibility limit of 2-line ferrihydrite within the first minute of observation and subsequently approach the solubility limit of goethite over time. As illustrated in Figure 1b, initial precipitation rates scale inversely to the pH. This is to be expected, as the degree of supersaturation with respect to both iron hydroxides stabilised is significantly higher at low pH. It is furthermore found that concentration measurements agree well across all emission lines considered. As measured iron concentrations drop continuously but remain close to the solubility limit of 2-line ferrihydrite, the stabilisation of goethite can be considered a dissolution-controlled process. Overall first order kinetics in the rate of iron precipitation furthermore suggest that the precipitation of 2-line ferrihydrite and goethite are competing processes, but do not involve particle-mediated growth mechanisms. In line with existing investigations into the precipitation pathways of α-FeOOH(s), transformation likely occurs via the dissolution of 2l-$Fe(OH)_3$(s) and re-precipitation from solution (Schwertmann, Stanjek et al. 2004, Soltis, Feinberg et al. 2016).

4. Conclusions and future outlook

This study has demonstrated that the formation of thermodynamically stable goethite is controlled by the redissolution of amorphous 2-line ferrihydrite. Due to the slow dissolution kinetics, aqueous iron concentrations remain in the order of 10^{-5} M within the first 30 minutes of equilibration, irrespective of the pH investigated. Given this progression, thermodynamic Gibbs free energy minimisation routines would hence underestimate the amount of iron at disposal to be transported across the concrete pore network. As the specific molar volume of 2-line ferrihydrite is more than 50% larger than that of goethite, the magnitude of internal stresses generated would moreover be underestimated. Aiming to accurately predict degree of structural deterioration over time, the evolution of aqueously dissolved [Fe] as well as the respective fractions of 2l-$Fe(OH)_3$(s) and α-FeOOH(s) present must be fitted by a set of pH dependent kinetic rate expressions that complement the existing thermodynamic modelling approach.

Acknowledgements

All XAS measurements were performed at the PHOENIX beamline at the Swiss Light Source, Paul Scherrer Institut, Villigen, Switzerland. The authors would like to thank Dr. Michael Plötze, Annette Röthlisberger and Marion Rothaupt for provision of the facility, valuable discussions and assistance with the XRD measurements presented in this study. The authors are furthermore grateful to the European Research Council (ERC) for the financial support provided under the European Union's Horizon 2020 research and innovation program (grant agreement no. 848794). The support from ETH Zurich internal Funding and NSF CMMI 1728358 helped enable the collaboration between ETH Zurich and Oregon State University.

References

Albert, C., O. B. Isgor and U. Angst (2022). "Literature-based data on pore solution compositions of cementitious systems."

Caruso, F., S. Mantellato, M. Palacios and R. J. Flatt (2017). "ICP-OES method for the characterization of cement pore solutions and their modification by polycarboxylate-based superplasticizers." Cement and Concrete Research 91: 52-60.

Furcas, F. E., B. Lothenbach, O. B. Isgor, S. Mundra, Z. Zhang and U. M. Angst (2022). "Solubility and speciation of iron in cementitious systems." Cement and Concrete Research 151: 106620.

Rzepa, G., G. Pieczara, A. Gaweł, A. Tomczyk and R. Zalecki (2016). "The influence of silicate on transformation pathways of synthetic 2-line ferrihydrite." Journal of Thermal Analysis and Calorimetry 125(1): 407-421.

Schwertmann, U. and R. M. Cornell (2008). Iron Oxides in the Laboratory: Preparation and Characterization, John Wiley & Sons.

Schwertmann, U., J. Friedl and H. Stanjek (1999). "From Fe (III) ions to ferrihydrite and then to hematite." Journal of Colloid and Interface Science 209(1): 215-223.

Schwertmann, U., H. Stanjek and H.-H. Becher (2004). "Long-term in vitro transformation of 2-line ferrihydrite to goethite/hematite at 4, 10, 15 and 25 C." Clay Minerals 39(4): 433-438.

Scrivener, K., R. Snellings and B. Lothenbach (2016). A practical guide to microstructural analysis of cementitious materials, Crc Press Boca Raton, FL, USA.

Soltis, J. A., J. M. Feinberg, B. Gilbert and R. L. Penn (2016). "Phase transformation and particle-mediated growth in the formation of hematite from 2-line ferrihydrite." Crystal Growth & Design 16(2): 922-932.

Thomas Arrigo, L. K., C. Mikutta, J. Byrne, K. Barmettler, A. Kappler and R. Kretzschmar (2014). "Iron and arsenic speciation and distribution in organic flocs from streambeds of an arsenic-enriched peatland." Environmental Science & Technology 48(22): 13218-13228.

Wieland, E., G. D. Miron, B. Ma, G. Geng and B. Lothenbach (2023). "Speciation of iron (II/III) at the iron-cement interface: a review." Materials and Structures 56(2): 31.

Zhu, M., C. Frandsen, A. F. Wallace, B. Legg, S. Khalid, H. Zhang, S. Mørup, J. F. Banfield and G. A. Waychunas (2016). "Precipitation pathways for ferrihydrite formation in acidic solutions." Geochimica et Cosmochimica Acta 172: 247-264.